*J. Fluid Mech.* (1994), *vol.* 261, *pp.* 75–93



# An estimate of the Kelvin impulse of a transient cavity

By J. P. BEST[1] AND J. R. BLAKE[2]

[1] Materials Research Laboratory (MRL) – DSTO, PO Box 50, Ascot Vale, Victoria, 3032, Australia

[2] School of Mathematics and Statistics, University of Birmingham, Edgbaston, Birmingham, B15 2TT, UK

(Received 9 April 1992 and in revised form 18 August 1993)

The Lagally theorem is used to obtain an expression for the Bjerknes force acting on a bubble in terms of the singularities of the fluid velocity potential, defined within the bubble by analytic continuation. This expression is applied to transient cavity collapse in the neighbourhood of boundaries, allowing analytical estimates to be made of the Kelvin impulse of the cavity. The known result for collapse near a horizontal rigid boundary is recovered, and the Kelvin impulse of a cavity collapsing in the neighbourhood of a submerged and partially submerged sphere is estimated. A numerical method is developed to deal with more general body shapes and in particular, bodies of revolution. Noting that the direction of the impulse at the end of the collapse phase generally indicates the direction of the liquid jet that may form, the behaviour of transient cavities in these geometries is predicted. In these examples the concept of a *zone of attraction* is introduced. This is a region around the body, within which the Kelvin impulse at the time of collapse, and consequent jet formation, is expected to be directed towards the body. Outside this zone the converse is true.

## 1. Introduction

Upon the collapse of a transient cavity in the neighbourhood of boundaries, a liquid jet is often observed to form and completely penetrate the bubble (Benjamin & Ellis 1966; Lauterborn & Bolle 1975; Vogel, Lauterborn & Timm 1989). Computations of the bubble shape are in agreement with these observations (Plesset & Chapman 1971; Guerri, Lucca & Prosperetti 1981; Blake, Taib & Doherty 1986). Significant attention has been paid to these jets as their impact against solid boundaries is a cause of cavitation damage. It is also evident that the pressure gradient induced by a gravitational field is a cause of jet formation such as, for example, occurs in the case of the bubble formed by an underwater explosion.

The concept of the Kelvin impulse was invoked by Benjamin & Ellis (1966) in order to explain the deformation from a spherical shape of a translating cavity, the formation of jets and the ultimate fate of the bubble as a vortex system. Subsequent to this, an approximate analytical expression for the Kelvin impulse of a cavity collapsing in an axisymmetric geometry near to a horizontal rigid boundary and in a uniform gravitational field has been derived by Blake *et al.* (1986). The evidence of the numerical computations presented in that paper indicates that the direction of the jet and the direction of the Kelvin impulse at the end of the bubble life are closely correlated. An analogous investigation of cavity collapse near a horizontal free surface (Blake, Taib & Doherty 1987) provided further evidence of this correlation.

In this paper, the theory of approximating the Kelvin impulse of a transient cavity is generalized to formally allow consideration of collapse in an arbitrary flow geometry. This theory utilizes the generalization of the Lagally theorem for multipoles and deformable bodies, given by Landweber & Miloh (1980). It is shown that the hydrodynamic force acting on a transient cavity is identically equal to zero, and this allows an expression to be obtained for the Bjerknes force exerted upon the bubble by the boundaries of the flow domain in terms of the strength of singularities of the velocity potential within the bubble, defined there by analytic continuation. Integration of this expression over the approximate lifetime of the bubble yields an estimate of the Kelvin impulse.

Particular geometries are then considered. In the first instance, the result of Blake *et al.* (1986) for the final Kelvin impulse of a cavity collapsing in the neighbourhood of a rigid boundary is recovered. Collapse near a stationary rigid sphere is a further example considered and one that may be treated exactly in the approximate theory. This latter example introduces the concept of a *zone of attraction*. Motion near a sphere in a uniform gravitational field is considered and the final Kelvin impulse estimated. A surface surrounding the sphere may be defined by the condition that the line through the point at which inception of the cavity occurs, in the direction of the final Kelvin impulse, is tangential to the sphere. On the basis of the proposition that the directions of the final Kelvin impulse and jet are closely correlated, this surface bounds a region within which, if motion occurs inside it, the jet will be directed towards the sphere upon collapse, and outside it the converse is true; hence the terminology, zone of attraction. By utilizing a linearized boundary condition at a horizontal free surface, the analysis is extended to consider a sphere submerged to its centreplane, and the zone of attraction is computed. In the penultimate section of the paper, a numerical method is described that allows consideration of transient cavity collapse in the neighbourhood of more general body shapes, and the particular class of shapes considered here is that of bodies of revolution. When the body is slender the results assume practical relevance in the context of the problem of underwater explosion bubble collapse near marine vessels.

## 2. The rate of change of the Kelvin impulse and the Lagally theorem

The fluid is considered ideal and the flow irrotational so a velocity potential, $\Phi$, may be introduced that satisfies Laplace's equation in the flow domain $\Omega$. The boundary of $\Omega$ is $\partial\Omega$ and $\partial\Omega \equiv S \cup \Sigma$ where $S$ is the surface of the bubble and $\Sigma$ consists of all other surfaces that bound $\Omega$. The unit normal to $\partial\Omega$ is denoted by $\boldsymbol{n}$ and considered to be directed exterior to $\Omega$.

The pressure within the bubble is assumed to be constant throughout the motion and equal to $p_c$. The hydrostatic pressure at the point of inception of the cavity is $p_\infty$. The lengthscale is $R_m$, of the order of the maximum bubble radius, and the timescale is $R_m(\rho/\Delta p)^{\frac{1}{2}}$, with $\rho$ the fluid density and $\Delta p = p_\infty - p_c$ the pressure scale. The gravitational field is uniform and given by $\boldsymbol{g} = -g\boldsymbol{e}_z$, with $\boldsymbol{e}_z$ an element of the set of Cartesian basis vectors. In non-dimensional variables, the Bernoulli equation evaluated at $S$ is

$$\frac{\partial \Phi}{\partial t} + \tfrac{1}{2}|\nabla\Phi|^2 + \delta^2 z - 1 = 0, \tag{2.1}$$

where

$$\delta = (\rho g R_m/\Delta p)^{\frac{1}{2}}, \tag{2.2}$$

is the buoyancy parameter.

The Kelvin impulse of a cavity is (scaled with respect to $R_m^3(\rho\Delta p)^{\frac{1}{3}}$)

$$\boldsymbol{I} = \oint_S \Phi \boldsymbol{n}\,\mathrm{d}S, \tag{2.3}$$

and $\boldsymbol{I}$ changes in response to the action of forces according to

$$\mathrm{d}\boldsymbol{I}/\mathrm{d}t = \boldsymbol{F}. \tag{2.4}$$

Integrating,

$$\boldsymbol{I}(t) = \boldsymbol{I}(0) + \int_0^t \boldsymbol{F}(t')\,\mathrm{d}t', \tag{2.5}$$

and $\boldsymbol{I}(0) = \boldsymbol{0}$, so having determined $\boldsymbol{F}$ the impulse may be computed. It should be noted that $\boldsymbol{F}$ is not the hydrodynamic force (the force acting on the bubble due to the pressure exerted by the fluid), which will be denoted by $\boldsymbol{F}_h$.

The rate of change of the Kelvin impulse is given by (Blake & Cerone 1982)

$$\mathrm{d}\boldsymbol{I}/\mathrm{d}t = \boldsymbol{F} = \boldsymbol{F}^{\Sigma} + \boldsymbol{F}^{g}, \tag{2.6}$$

with

$$\boldsymbol{F}^{\Sigma} = \int_{\Sigma} \left\{ \tfrac{1}{2}|\nabla\Phi|^2 \boldsymbol{n} - \frac{\partial\Phi}{\partial n}\nabla\Phi \right\} \mathrm{d}S, \tag{2.7}$$

and

$$\boldsymbol{F}^{g} = \delta^2 V \boldsymbol{e}_z. \tag{2.8}$$

$\boldsymbol{F}^{g}$ is the buoyancy force and $\boldsymbol{F}^{\Sigma}$ the Bjerknes force exerted by the boundary. Equivalently, the integration in (2.7) may be considered as over the bubble surface $S$, in which case (Blake & Cerone 1982)

$$\boldsymbol{F}^{\Sigma} = -\oint_S \left\{ \tfrac{1}{2}|\nabla\Phi|^2 \boldsymbol{n} - \frac{\partial\Phi}{\partial n}\nabla\Phi \right\} \mathrm{d}S. \tag{2.9}$$

It is worthwhile to consider the relationship between the above expressions and the Lagally theorem. The hydrodynamic force on a bubble is

$$\boldsymbol{F}_h = \oint_S p\boldsymbol{n}\,\mathrm{d}S, \tag{2.10}$$

and provided $p$ is uniform over $S$, this is identically equal to zero! In the case of the transient cavity considered here, this is indeed the case as the pressure within the bubble is constant throughout the motion. In view of this, it is a routine matter to derive (2.6). The hydrodynamic force on a body, whose boundary is $S$, is given in general terms by (Newman 1977)

$$\boldsymbol{F}_h = -\frac{\mathrm{d}\boldsymbol{I}}{\mathrm{d}t} - \oint_S \left\{ \tfrac{1}{2}|\nabla\Phi|^2 \boldsymbol{n} - \frac{\partial\Phi}{\partial n}\nabla\Phi \right\} \mathrm{d}S + \delta^2 V \boldsymbol{e}_z. \tag{2.11}$$

If this force is identically equal to zero then (2.6), (2.8) and (2.9) follow immediately.

The Lagally theorem follows when the first two terms on the right-hand side of (2.11) are evaluated in terms of the singularities, within the volume bounded by $S$, of the potential defined there by analytic continuation. Landweber & Miloh (1980) have generalized the Lagally theorem to treat deformable bodies, and those for which the velocity potential within the body has multipole singularities. In the course of their derivation, Landweber & Miloh (1980) establish the following expression:

$$\oint_S \left\{ \tfrac{1}{2}|\nabla\Phi|^2 \boldsymbol{n} - \frac{\partial\Phi}{\partial n}\nabla\Phi \right\} \mathrm{d}S = 4\pi \sum_s P_q D_s^q (\nabla\phi')_s. \tag{2.12}$$

In deriving this result, the potential defined within the volume bounded by $S$ is singular at points whose position vectors are $\boldsymbol{r}_s \equiv (x_s, y_s, z_s)$. In the neighbourhood of the singularity, the potential is written as

$$\Phi = \phi + \phi', \tag{2.13}$$

where $\phi'$ is regular, and $\phi$ is of the form

$$\phi = -P_q D_s^q(1/R), \quad D_s^q = \frac{\partial^q}{\partial x_s^\alpha \partial y_s^\beta \partial z_s^\gamma}, \quad R^2 = (x-x_s)^2+(y-y_s)^2+(z-z_s)^2, \tag{2.14}$$

where the summation convention has been used over $q$, the order of the multipole, and for each $q$ the sum is taken over all $\alpha, \beta, \gamma$ such that $\alpha+\beta+\gamma = q$. In (2.12), $\sum_s$ denotes summation over all singularities within $S$, and $(\,)_s$ denotes evaluation at the singularity $s$; $\boldsymbol{r} \equiv (x, y, z)$ is the position vector of an arbitrary point in space. In comparing (2.12) with equation (24) of Landweber & Miloh (1980), note that the normal used in that paper is directed oppositely from that used here.

Using (2.12) in (2.9) gives the Bjerknes force as

$$\boldsymbol{F}^{\Sigma} = -4\pi \sum_s P_q D_s^q (\nabla \phi')_s, \tag{2.15}$$

which is the required expression in terms of the strength of the singularities of $\Phi$ within $S$, and derivatives of the regular part of the fluid velocity at these singularities.

## 3. General theory for estimating the Kelvin impulse of a transient cavity

In what follows the small parameter $\epsilon$ is defined to be $O(1/\xi)$, where $\xi$ is a typical distance from the bubble centroid to $\Sigma$, and the geometry of $\Sigma$ is considered to be time independent. It is further assumed that the buoyancy parameter $\delta$ is $O(\epsilon)$. The radial coordinate of the bubble surface is of the form

$$a(\theta, \phi, t) = R(t) + \sum_{l=1}^{\infty} \sum_{m=0}^{l} \alpha_{l,m}(t) \mathscr{P}_l^m(\cos\theta) \cos(m\phi + \omega_{l,m}(t)), \tag{3.1}$$

where $\mathscr{P}_l^m$ is an associated Legendre function (Gradshteyn & Ryzhik 1979). This paper is concerned with the lowest-order perturbations to the infinite-fluid behaviour caused by buoyancy and nearby boundaries. The potential in the neighbourhood of the bubble may be written in the form of (2.13). Transient cavity motion in an infinite fluid has been considered by Rayleigh (1917), with the potential due to such motion represented by a time-dependent source located at the centre of the bubble. This behaviour is perturbed by buoyancy and nearby boundaries, so the leading-order contribution to $\Phi$ is a source term, and as a matter of notation let $P_0$ in (2.14) be written as $m/4\pi$, with $m$ the source strength and $|P_0|$ is $O(1)$. The perturbing influence of both buoyancy and nearby boundaries has been considered by Herring (1950). The bubble is perturbed from a spherical shape throughout its growth and collapse and the lowest-order correction to a spherical form is merely a translation of the sphere as a whole. In view of this analysis, it is inferred that the leading contribution to $|P_1|$ is $O(\epsilon^2)$, with the other $P_q$ of higher order. The term $\phi'$ in (2.13) is non-zero owing to the presence of the boundary $\Sigma$. This contribution to the potential may be considered as due to images, exterior to $\Omega$, of the singularities within the bubble, and is $O(\epsilon)$. Furthermore, the terms $\alpha_{1,m}$ in (3.1), that are non-zero owing to departures from the spherical shape, are $O(\epsilon^2)$.

These mathematical features are characteristic of the perturbing influence of both nearby boundaries and buoyancy.

Applying (2.15), the Bjerknes force may be written as

$$\boldsymbol{F}^{\Sigma} = -m\nabla\phi'(\boldsymbol{r}_c) + O(\epsilon^4), \tag{3.2}$$

where $\boldsymbol{r}_c$ is the position vector of the bubble centroid and it is remarked that the leading term in this expression is $O(\epsilon^2)$. The buoyancy force is

$$\boldsymbol{F}^{g} = \tfrac{4}{3}\pi\delta^2 R^3 \boldsymbol{e}_z + O(\epsilon^4), \tag{3.3}$$

since the terms $\alpha_{1,m}$ in (3.1) do not contribute in evaluation of the volume.

To proceed further set

$$\phi' = -\frac{m}{4\pi} g(\boldsymbol{r}, \boldsymbol{r}_c, \boldsymbol{s}) + O(\epsilon^2), \tag{3.4}$$

where $g$ is a function of $\boldsymbol{r}, \boldsymbol{r}_c$ and $\boldsymbol{s} \equiv (s_1, s_2, \ldots, s_n)$, which is a set of time-independent distance parameters that characterize the geometry of $\Sigma$. Hence

$$\begin{aligned} \boldsymbol{F}^{\Sigma} &= \frac{m^2}{4\pi} \nabla_r g(\boldsymbol{r}_0, \boldsymbol{s}) + O(\epsilon^4), \\ &= \frac{m^2}{16\pi} \boldsymbol{\Gamma} + O(\epsilon^4), \end{aligned} \tag{3.5}$$

where $\boldsymbol{r}_0$ is the position of the bubble centroid at $t = 0$. Equation (3.5) defines $\boldsymbol{\Gamma}$ as a function of $\boldsymbol{r}_0$ and $\boldsymbol{s}$ that is $O(\epsilon^2)$. Note that $\boldsymbol{\Gamma}$ is defined in terms of $\boldsymbol{r}_0$, as $\dot{\boldsymbol{r}}_c$ relates to $P_1$ (or dipole) contributions to the potential that arise owing to migration of the bubble, and since these are $O(\epsilon^2)$ the time variation of $\boldsymbol{r}_c$ contributes to $\boldsymbol{F}^{\Sigma}$ to $O(\epsilon^4)$. As a further consequence of this, $\boldsymbol{r}_c$ may be routinely replaced by $\boldsymbol{r}_0$ in (3.2) and (3.4), and this is done in the examples considered later in this paper.

Application of the kinematic boundary condition at the surface of the bubble determines the source strength $m$. This condition is that

$$\frac{\partial \Phi}{\partial n} = \frac{\mathrm{d}\boldsymbol{x}}{\mathrm{d}t} \cdot \boldsymbol{n}, \tag{3.6}$$

where $\partial\Phi/\partial n$ is the normal fluid velocity and $\mathrm{d}\boldsymbol{x}/\mathrm{d}t$ is the velocity of a Lagrangian surface particle. Using (3.1) to evaluate the right-hand side of (3.6), and (2.13) to evaluate the left-hand side, yields

$$m = 4\pi R^2 \dot{R} + O(\epsilon^2), \tag{3.7}$$

so

$$\boldsymbol{F}^{\Sigma} = \pi R^4 \dot{R}^2 \boldsymbol{\Gamma} + O(\epsilon^4). \tag{3.8}$$

In order to integrate (3.3) and (3.8) with respect to time to determine an approximation to the impulse, an expression is required for $R(t)$. This is obtained from the Bernoulli equation, evaluated at the bubble surface (equation (2.1)). Substituting into this expression using (2.13) and (3.7) yields

$$R\ddot{R} + \tfrac{3}{2}\dot{R}^2 - \frac{\partial \phi'}{\partial t}(\boldsymbol{r}_0, \boldsymbol{s}) + 1 + O(\epsilon^2) = 0. \tag{3.9}$$

Utilizing (3.4), and noting that any time dependence of $\boldsymbol{r}_c$ contributes to $\partial\phi'/\partial t$ to $O(\epsilon^4)$, (3.9) becomes

$$R\ddot{R} + \tfrac{3}{2}\dot{R}^2 + \mu R(R\ddot{R} + 2\dot{R}^2) + 1 = 0, \tag{3.10}$$

with the error of $O(\epsilon^2)$, and

$$\mu = g(\boldsymbol{r}_0, s) \tag{3.11}$$

is $O(\epsilon)$. Equivalently, (3.10) could be obtained via an energy argument. Note that to this order of computation, the equation giving $R(t)$ is independent of $\delta$. Multiplying (3.10) by the integrating factor $R^2$ gives

$$\frac{\mathrm{d}}{\mathrm{d}R}[\tfrac{1}{2}R^3\dot{R}^2(1+\mu R)]+R^2=0. \tag{3.12}$$

At the maximum radius $R=1$, $\dot{R}=0$, so integration yields

$$\dot{R}=\begin{cases}\sqrt{\frac{2}{3}}(1-R^3)^{\frac{1}{2}}R^{-\frac{3}{2}}(1+\mu R)^{-\frac{1}{2}}, & 0\leqslant t\leqslant \tfrac{1}{2}T,\\ -\sqrt{\frac{2}{3}}(1-R^3)^{\frac{1}{2}}R^{-\frac{3}{2}}(1+\mu R)^{-\frac{1}{2}}, & \tfrac{1}{2}T\leqslant t\leqslant T,\end{cases} \tag{3.13}$$

with the sign of the square root of $\dot{R}^2$ appropriately chosen according to whether the bubble is expanding ($0\leqslant t\leqslant \frac{1}{2}T$) or collapsing ($\frac{1}{2}T\leqslant t\leqslant T$). The symmetry of the motion about the maximum radius which occurs at $t=\frac{1}{2}T$ is noted, with $T$ the period of the motion.

To proceed, $R(t)$ is determined implicitly and the Kelvin impulse then evaluated. Now

$$\begin{aligned} t&=\int_0^t \mathrm{d}t'=\int_0^R \mathrm{d}R'/\dot{R},\\ &=\begin{cases}\sqrt{\frac{3}{2}}\displaystyle\int_0^R (1-R'^3)^{-\frac{1}{2}}R'^{\frac{3}{2}}(1+\tfrac{1}{2}\mu R')\,\mathrm{d}R', & 0\leqslant t\leqslant \tfrac{1}{2}T,\\ \sqrt{\frac{3}{2}}\left\{\displaystyle\int_0^1-\int_1^R\right\}(1-R'^3)^{-\frac{1}{2}}R'^{\frac{3}{2}}(1+\tfrac{1}{2}\mu R')\,\mathrm{d}R' & \tfrac{1}{2}T\leqslant t\leqslant T,\end{cases}\end{aligned} \tag{3.14}$$

where, in accord with the order of the approximation, a binomial expansion of $(1+\mu R')^{\frac{1}{2}}$ has been utilized. Making the transformation $\alpha'=R'^3$ ($\alpha=R^3$), (3.14) is written in terms of incomplete ($B_\alpha(w,z)$) and complete ($B(w,z)$) Beta-functions (Abramowitz & Stegun 1965):

$$t=\begin{cases}(1/\sqrt{6})[B_\alpha(\frac{5}{6},\frac{1}{2})+\frac{1}{2}\mu B_\alpha(\frac{7}{6},\frac{1}{2})], & 0\leqslant t\leqslant \tfrac{1}{2}T,\\ (2/\sqrt{6})[B(\frac{5}{6},\frac{1}{2})+\frac{1}{2}\mu B(\frac{7}{6},\frac{1}{2})]\\ \quad -(1/\sqrt{6})[B_\alpha(\frac{5}{6},\frac{1}{2})+\frac{1}{2}\mu B_\alpha(\frac{7}{6},\frac{1}{2})], & \tfrac{1}{2}T\leqslant t\leqslant T.\end{cases} \tag{3.15}$$

At $t=T$, $\alpha=0$, so the period is given by

$$T=(2/\sqrt{6})[B(\tfrac{5}{6},\tfrac{1}{2})+\tfrac{1}{2}\mu B(\tfrac{7}{6},\tfrac{1}{2})]. \tag{3.16}$$

Using (3.8), the Kelvin impulse caused by $\Sigma$ is

$$\boldsymbol{I}=\pi\boldsymbol{\Gamma}\int_0^t R^4\dot{R}^2\,\mathrm{d}t'=\pi\boldsymbol{\Gamma}\int_0^R R'^4\dot{R}\,\mathrm{d}R', \tag{3.17}$$

and using (3.13) and a substitution as above to carry out the integration yields

$$\boldsymbol{I}^{\Sigma}(t)=\begin{cases}(\sqrt{6\pi}/9)\,\boldsymbol{\Gamma}[B_\alpha(\frac{7}{6},\frac{3}{2})-\frac{1}{2}\mu B_\alpha(\frac{3}{2},\frac{3}{2})], & 0\leqslant t\leqslant \tfrac{1}{2}T,\\ (2\sqrt{6\pi}/9)\,\boldsymbol{\Gamma}[B(\frac{7}{6},\frac{3}{2})-\frac{1}{2}\mu B(\frac{3}{2},\frac{3}{2})]\\ \quad -(\sqrt{6\pi}/9)\,\boldsymbol{\Gamma}[B_\alpha(\frac{7}{6},\frac{3}{2})-\frac{1}{2}\mu B_\alpha(\frac{3}{2},\frac{3}{2})], & \tfrac{1}{2}T\leqslant t\leqslant T,\end{cases} \tag{3.18}$$

with an error of $O(\epsilon^4)$. A similar evaluation yields the impulse due to buoyancy as

$$\boldsymbol{I}^g(t) = \begin{cases} (2\sqrt{6\pi}/9)\,\delta^2[B_\alpha(\frac{11}{6},\frac{1}{2}) + \frac{1}{2}\mu B_\alpha(\frac{13}{6},\frac{1}{2})]\,\boldsymbol{e}_z, & 0 \leqslant t \leqslant \frac{1}{2}T, \\ (4\sqrt{6\pi}/9)\,\delta^2[B(\frac{11}{6},\frac{1}{2}) + \frac{1}{2}\mu B(\frac{13}{6},\frac{1}{2})]\,\boldsymbol{e}_z \\ \quad -(2\sqrt{6\pi}/9)\,\delta^2[B_\alpha(\frac{11}{6},\frac{1}{2}) + \frac{1}{2}\mu B_\alpha(\frac{13}{6},\frac{1}{2})]\,\boldsymbol{e}_z, & \frac{1}{2}T \leqslant t \leqslant T, \end{cases} \tag{3.19}$$

with an error of $O(\epsilon^4)$.

In order to estimate the period and Kelvin impulse of a transient cavity, the coefficients $\mu$ and $\boldsymbol{\Gamma}$ must be evaluated. These are purely functions of the geometry of $\Sigma$ and thus characterize its influence upon the motion of the cavity. Several examples in the next sections illustrate the approach.

## 4. Examples treated exactly in the approximate theory

### 4.1. *Collapse near a horizontal rigid plane*

Consider transient cavity collapse near a horizontal rigid plane at $z = 0$. The regular potential in the neighbourhood of the bubble, to $O(\epsilon)$, is due to an image source of strength $m$ reflected about the plane. Considering inception of the cavity to occur at $\boldsymbol{r}_0 \equiv (0, 0, \xi)$,

$$\phi'(\boldsymbol{r}) = -\frac{m}{4\pi} g(\boldsymbol{r}, \boldsymbol{r}_0), \tag{4.1}$$

with

$$g(\boldsymbol{r}, \boldsymbol{r}_0) = \frac{1}{|\boldsymbol{r} - (0, 0, -\xi)|}. \tag{4.2}$$

From (4.2) $\boldsymbol{\Gamma}$ and $\mu$ are evaluated as

$$\boldsymbol{\Gamma} = -\frac{1}{\xi^2}\boldsymbol{e}_\xi, \quad \mu = \frac{1}{2|\xi|}, \tag{4.3}$$

where $\boldsymbol{e}_\xi$ is a unit vector directed away from the boundary. Blake *et al.* (1986) did not consider the correction to the Rayleigh equation for $R$ due to the nearby boundary, so to recover the result of that paper $\mu$ is set equal to zero in (3.18) and (3.19).

Since the Kelvin impulse is the impulse that would have to be applied over the surface of the bubble in order to generate the observed flow field from rest, there is some physical basis for supposing that the direction of the jet and the direction of the Kelvin impulse at the time of collapse are closely correlated. The analytical estimates of the impulse at the end of the bubble collapse obtained by Blake *et al.* (1986, 1987) were found to provide reasonable estimates of the Kelvin impulse of the jet-pierced bubble, despite the analysis assuming small departures from a spherical shape. This follows from the speed with which jet formation occurs. Typically, the time over which this non-spherical collapse occurs is of the order of 2–3 % of the bubble life. Over some interval, $\Delta t$, the change in the Kelvin impulse is

$$\Delta \boldsymbol{I} = \int_t^{t+\Delta t} \boldsymbol{F}(t')\,\mathrm{d}t', \tag{4.4}$$

so that

$$|\Delta \boldsymbol{I}| \leqslant \Delta t \sup_{(t, t+\Delta t)} |\boldsymbol{F}(t)|, \tag{4.5}$$

where sup denotes the supremum value. $\boldsymbol{F}$ is bounded throughout the motion so that, over a sufficiently small time interval, the magnitude of the impulse change is small.

The time at which the bubble enters the rapid collapse phase and becomes highly non-spherical is given with good accuracy by (3.16), and up until this time the Kelvin impulse can be determined using the results of §3. Because of the generally short time, $\Delta t$, over which the collapse occurs, this provides a reliable estimate of the impulse of the non-spherical collapsed bubble, the change in the impulse brought about by the deformation from a spherical shape being small, in accord with (4.5).

### 4.2. *Collapse near a stationary rigid sphere*

Without loss of generality, suppose that the centre of a fixed rigid sphere of radius $a$ is located at the origin and that inception occurs at $z = \xi$. In this case $\phi'$ is given by the Weiss sphere theorem (see Milne-Thomson 1960)

$$\phi'(\boldsymbol{r}) = -\frac{am}{4\pi\xi}\frac{1}{|\boldsymbol{r}-(0,0,a^2/\xi)|}+\frac{m}{4\pi a}\int_0^{a^2/\xi}\frac{\mathrm{d}\nu}{|\boldsymbol{r}-(0,0,\nu)|}. \tag{4.6}$$

The first term corresponds to a source of strength $am/\xi$ located at $z = a^2/\xi$, and the second term to a uniform linear distribution of sinks of density $m/a$, from $z = 0$ to $z = a^2/\xi$. This is the image set associated with a source located at $z = \xi$ and is such that the boundary condition $\nabla\Phi\cdot\boldsymbol{n} = 0$ is satisfied at the surface of the sphere. In this example the geometry of $\Sigma$ is characterized by $s \equiv a$. From (4.6)

$$g(\boldsymbol{r}, \boldsymbol{r}_0, s) = \frac{a}{\xi}\frac{1}{|\boldsymbol{r}-(0,0,a^2/\xi)|}-\frac{1}{a}\int_0^{a^2/\xi}\frac{\mathrm{d}\nu}{|\boldsymbol{r}-(0,0,\nu)|}, \tag{4.7}$$

and

$$\boldsymbol{\Gamma} = -\frac{4a^3}{\xi(\xi^2-a^2)^2}\boldsymbol{e}_r, \quad \mu = \frac{a}{\xi^2-a^2}-\frac{1}{a}\ln\left(\frac{\xi^2}{\xi^2-a^2}\right), \tag{4.8}$$

where the only non-zero component of the Bjerknes force exerted by the sphere is directed towards the origin, as denoted by use of the radial vector $\boldsymbol{e}_r$.

Since the direction of the Kelvin impulse at the conclusion of the collapse is expected to be closely correlated with the direction of the jet, the theory developed here may be used to infer the behaviour of buoyant cavities collapsing in the neighbourhood of a sphere. The angle, $\psi$, that the direction of the final impulse makes with the line joining the point of inception to the centre of the sphere is

$$\psi = \arctan\left(I_\theta(T_c)/I_r(T_c)\right), \tag{4.9}$$

where $I_\theta$ and $I_r$ are the components of the Kelvin impulse in spherical coordinates. The geometry is shown in figure 1. The critical angle, $\psi_c$, is defined by

$$\psi_c = \arcsin\left(a/\xi\right), \tag{4.10}$$

and

$$\psi = \psi_c \tag{4.11}$$

defines a condition such that the direction of the final Kelvin impulse is tangential to the sphere. Since $\boldsymbol{I}(T_c)$ is a function of $\xi$ and $\theta$, (4.11) defines a surface surrounding the sphere and this surface shall be hereafter denoted by $S_a$. Within this surface the Bjerknes attraction of the sphere is sufficiently large that the final Kelvin impulse is directed towards it. It is supposed that the jet formed will be similarly directed. Thus the terminology *zone of attraction* is introduced to describe this region of space. Conversely, outside the surface defined by (4.11), the final Kelvin impulse is directed away from the sphere.

The example $a = 2.0$, $\delta = 0.1$ is shown in figure 2. Equation (4.11) has been solved

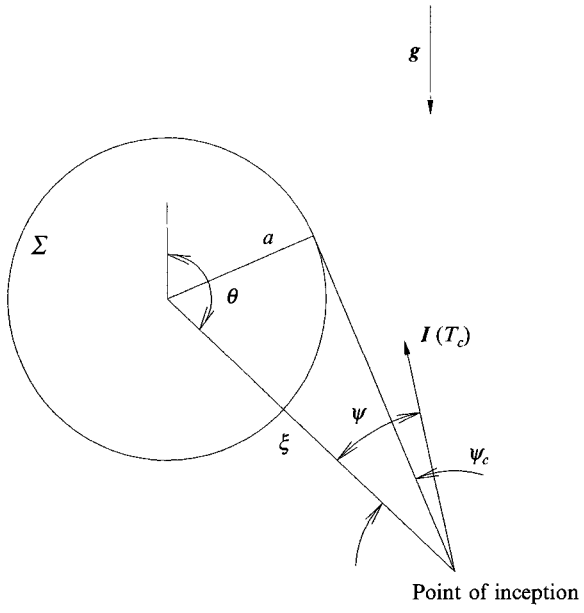


FIGURE 1. The geometry for buoyant cavity motion near a stationary, rigid sphere.

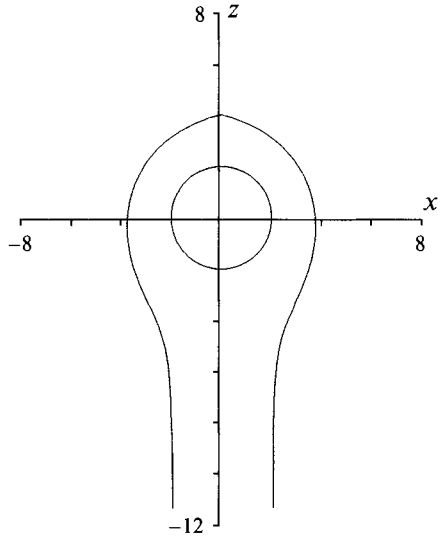


FIGURE 2. The zone of attraction around a sphere of radius $a = 2.0$.
The buoyancy parameter is $\delta = 0.1$.

by the bisection method, with substitution of (4.8) into (3.18) and (3.19) yielding the appropriate components of the impulse. $S_a$ encloses the sphere and as $z \to -\infty$ the section of this surface in some plane $z$ = constant tends to $x^2 + y^2 = a^2$. This is expected on physical grounds. As $z \to -\infty$ the presence of the sphere is little felt ($\Gamma, \mu \to 0$) so the dominant buoyancy force yields a final Kelvin impulse directed upwards and towards the sphere, if the point of inception is under it.

In regard to jet formation as a damage-causing mechanism, the zone of attraction is relevant as it defines a region in which jet impact may occur. However, the part of

this zone extending to $z = -\infty$ is of little relevance in this context as a jet forming towards the sphere, but a long way from it, will cause no damage.

4.3. *Collapse near a stationary sphere, submerged to its centreplane at a free surface*

Consider now a sphere submerged to its centreplane at a horizontal free surface defined by $z = 0$. To the accuracy of computation required, the linearized boundary condition that the potential vanishes on the free surface is applied. For the purpose of calculation of $\Gamma$, axisymmetry may be exploited and the point of inception considered as

$$\boldsymbol{r}_0 = (\omega, 0, \zeta), \tag{4.12}$$

with the centre of the sphere the origin. The distance between the point of inception and the sphere centre is

$$\xi = (\omega^2 + \zeta^2)^{\frac{1}{2}}. \tag{4.13}$$

The simplest way to satisfy the boundary condition on $z = 0$ is to introduce an image sink of strength $m$ at

$$\boldsymbol{r}_i = (\omega, 0, -\zeta), \tag{4.14}$$

which is the reflection of $\boldsymbol{r}_0$ about the plane $z = 0$, and determine $\Phi$ such that $\nabla\Phi \cdot \boldsymbol{n} = 0$ on the whole of the sphere surface. From symmetry considerations, it is evident that the resultant potential will satisfy $\Phi = 0$ on $z = 0$.

The sphere theorem may be applied to both the source representing the bubble and its image sink to give

$$\begin{aligned}\phi'(\boldsymbol{r}) = {} & \frac{m}{4\pi}\frac{1}{|\boldsymbol{r}-(\omega,0,-\zeta)|} \\ & -\frac{am}{4\pi\xi}\frac{1}{|\boldsymbol{r}-(a^2\omega/\xi^2, 0, a^2\zeta/\xi^2)|} + \frac{m}{4\pi a}\int_0^{a^2/\xi}\frac{\mathrm{d}\nu}{|\boldsymbol{r}-(\nu\omega/\xi, 0, \nu\zeta/\xi)|} \\ & +\frac{am}{4\pi\xi}\frac{1}{|\boldsymbol{r}-(a^2\omega/\xi^2, 0, -a^2\zeta/\xi^2)|} - \frac{m}{4\pi a}\int_0^{a^2/\xi}\frac{\mathrm{d}\nu}{|\boldsymbol{r}-(\nu\omega/\xi, 0, -\nu\zeta/\xi)|}.\end{aligned} \tag{4.15}$$

$\Gamma$ and $\mu$ are

$$\Gamma = \Gamma_r \boldsymbol{e}_r + \Gamma_z \boldsymbol{e}_z, \tag{4.16}$$

$$\Gamma_r = -\frac{4a^3\omega}{\xi^2(\xi^2-a^2)^2} + \frac{2}{a\omega}\left\{\frac{4a^2\omega^2\xi^2 - (a^2+\xi^2)(\xi^4+a^4+2a^2\zeta^2)}{(\xi^4+a^4+2a^2(\zeta^2-\omega^2))^{\frac{3}{2}}} + 1\right\}, \tag{4.17}$$

$$\Gamma_z = -\frac{4a^3\zeta}{\xi^2(\xi^2-a^2)^2} + \frac{2}{a\zeta}\left\{\frac{4a^2\zeta^2\xi^2 - (a^2-\xi^2)(\xi^4+a^4-2a^2\omega^2)}{(\xi^4+a^4+2a^2(\zeta^2-\omega^2))^{\frac{3}{2}}} - 1\right\} + \frac{\operatorname{sgn}(\zeta)}{\zeta^2}, \tag{4.18}$$

$$\begin{aligned}\mu = {} & -\frac{1}{2|\zeta|} + \frac{a}{\xi^2-a^2} - \frac{1}{a}\ln\left\{\frac{\xi^2}{\xi^2-a^2}\right\} \\ & -\frac{a}{(\xi^4+a^4+2a^2(\zeta^2-\omega^2))^{\frac{1}{2}}} + \frac{1}{a}\ln\left\{\frac{(\xi^4+a^4+2a^2(\zeta^2-\omega^2))^{\frac{1}{2}} + a^2 + \zeta^2 - \omega^2}{\xi^2+\zeta^2-\omega^2}\right\},\end{aligned} \tag{4.19}$$

where $\boldsymbol{e}_r$ and $\boldsymbol{e}_z$ are cylindrical basis vectors.

The zone of attraction is defined by the condition that the line passing through the point of inception, in the direction of the final Kelvin impulse, is tangential to the surface of the sphere. The equation of this line is

$$r' = \omega + \lambda I_r(T_c), \quad z' = \zeta + \lambda I_z(T_c), \tag{4.20}$$

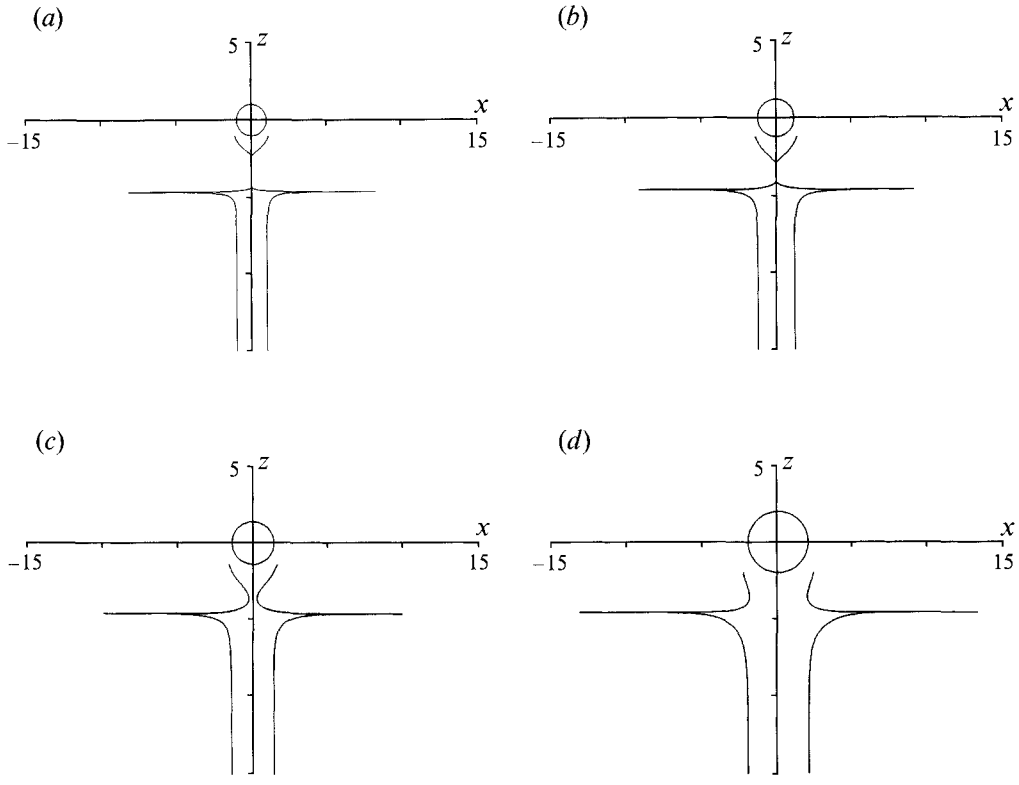


FIGURE 3. The zone of attraction around a sphere submerged to its centreplane at a free surface. The cross-section through the axis of symmetry is shown. $\delta = 0.1$. The radius of the sphere is (*a*) $a = 1.0$, (*b*) $a = 1.2$, (*c*) $a = 1.4$, (*d*) $a = 2.0$.

where $\lambda$ is a parameter and the components of the final Kelvin impulse are functions of $\omega$ and $\zeta$, which define the point of inception. The equation defining the surface of the sphere is

$$r'^2 + z'^2 = a^2, \tag{4.21}$$

so that the points at which the line and sphere intersect are given by the solutions of

$$(I_r^2(T_c) + I_z^2(T_c))\,\lambda^2 + 2(\omega I_r(T_c) + \zeta I_z(T_c))\,\lambda + (\xi^2 - a^2) = 0. \tag{4.22}$$

For the line to be tangential to the sphere this equation has only one solution, so the equation defining the surface, $S_a$, that bounds the zone of attraction, is

$$f(\omega, \zeta) = (\omega I_r(T_c) + \zeta I_z(T_c))^2 - (I_r^2(T_c) + I_z^2(T_c))\,(\xi^2 - a^2) = 0. \tag{4.23}$$

This function is negative outside the zone of attraction and positive inside it. Utilizing this fact, (4.23) has been here solved using the bisection method. Note also that for the solution to be physically relevant $\lambda$ must be positive, indicating that the impulse is directed towards the sphere.

Examples are shown for $\delta = 0.1$ and various values of $a$ in figure 3. The section through $S_a$ in the axis of symmetry is shown for $a = 1.0$ (figure 3*a*), $a = 1.2$ (figure 3*b*), $a = 1.4$ (figure 3*c*) and $a = 2.0$ (figure 3*d*). Consider first $a = 1.0$. The striking feature is that the zone of attraction consists of two distinct regions. This may be explained by considering the forces acting on the bubble. In close proximity to the sphere its Bjerknes attraction is dominant causing the jet to be directed towards it, noting that the effect of the free surface is to cause jet formation downwards. As the point of

inception moves downwards, the Bjerknes force exerted by the sphere falls, and the effect of the free surface becomes dominant and the final Kelvin impulse is directed away from the sphere. At greater depths the free surface and Bjerknes force exerted by the sphere are little felt, and buoyancy causes jet formation upwards and towards the sphere. As $z \to -\infty$ the section of $S_a$ in the plane $z =$ constant tends to that of the sphere in the plane $z = 0$.

A further significant feature is that the bottom section of the zone exhibits a branch that tends outwards and is asymptotic to the plane defined by

$$2\delta^2\left[B(\tfrac{11}{16},\tfrac{1}{2})+\frac{1}{4z}B(\tfrac{13}{6},\tfrac{1}{2})\right]-\frac{1}{z^2}\left[B(\tfrac{7}{6},\tfrac{3}{2})-\frac{1}{4z}B(\tfrac{3}{2},\tfrac{3}{2})\right]=0. \tag{4.24}$$

The significance of this plane is that in the absence of the sphere, it defines that depth of inception at which the final vertical component of the Kelvin impulse is zero in the approximate theory. In this case, for $\omega$ sufficiently large, just below the surface defined by (4.24) there is a small upwards component of the impulse that combines with the small component parallel to the free surface and due to the presence of the sphere, in order that the final impulse is directed towards the sphere. Note also that the part of $S_a$ near to the sphere is only calculated to some close point, as the theory is not applicable in the very close neighbourhood of its surface.

The changing structure of the zone of attraction as $a$ increases is interesting and the sequence shown in figure 3 illustrates this. For $a = 1.2$ the larger sphere causes a greater Bjerknes force so that part of the zone of attraction immediately below the sphere extends to a greater depth. Figure 3(*c*) ($a = 1.4$) illustrates the merging of the upper and lower portions of the zone of attraction. In this case the sphere is sufficiently large that, near to the $z$-axis at least, there is no region where the repulsion of the free surface is dominant. The example of $a = 2.0$ (figure 3*d*) shows that for a sphere reasonably larger than the bubble, the free surface is significant only at the edges of the sphere.

## 5. The numerical method

To exploit the full power of the theory developed here for estimating the Kelvin impulse of a transient cavity, it is necessary to investigate numerical methodologies for dealing with complicated flow field geometries. In order to evaluate the approximation to the Kelvin impulse, suppose that the regular part of the potential in the neighbourhood of the bubble centroid is considered as due to a distribution of sources of surface density $m\sigma$, over $\Sigma$. Then

$$\phi'(\boldsymbol{r}) = -\frac{m}{4\pi}g(\boldsymbol{r},\boldsymbol{r}_0,s) \tag{5.1}$$

with

$$g(\boldsymbol{r},\boldsymbol{r}_0,s) = \int_\Sigma \frac{\sigma(\boldsymbol{q},\boldsymbol{r}_0,s)}{|\boldsymbol{r}-\boldsymbol{q}|}\mathrm{d}S(\boldsymbol{q}). \tag{5.2}$$

Hence

$$\boldsymbol{I} = -4\int_\Sigma \frac{\sigma(\boldsymbol{q},\boldsymbol{r}_0,s)\,(\boldsymbol{r}_0-\boldsymbol{q})}{|\boldsymbol{r}_0-\boldsymbol{q}|^3}\mathrm{d}S(\boldsymbol{q}), \tag{5.3}$$

and

$$\mu = \int_\Sigma \frac{\sigma(\boldsymbol{q},\boldsymbol{r}_0,s)}{|\boldsymbol{r}_0-\boldsymbol{q}|}\mathrm{d}S(\boldsymbol{q}). \tag{5.4}$$

Note that $\sigma$ depends upon the position on $\Sigma$ (the vector $\boldsymbol{q}$), the vector $s$ that characterizes the geometry of $\Sigma$, and the point of inception $\boldsymbol{r}_0$.

Writing

$$\Phi = -\frac{m}{4\pi}\frac{1}{|\boldsymbol{r}-\boldsymbol{r}_0|}+\phi'(\boldsymbol{r}), \tag{5.5}$$

and restricting attention to cases where $\Sigma$ is rigid, the boundary condition

$$\nabla\Phi(\boldsymbol{p})\cdot\boldsymbol{n}(\boldsymbol{p}) = 0, \tag{5.6}$$

satisfied for all $\boldsymbol{p}\in\Sigma$, determines $\sigma(\boldsymbol{q}, \boldsymbol{r}_0, s)$. Using (5.5) in (5.6), the following integral equation is obtained for $\sigma$:

$$\sigma(\boldsymbol{p}, \boldsymbol{r}_0, s) = \frac{1}{2\pi}\frac{(\boldsymbol{p}-\boldsymbol{r}_0)\cdot\boldsymbol{n}(\boldsymbol{p})}{|\boldsymbol{p}-\boldsymbol{r}_0|^3}+\frac{1}{2\pi}\int_\Sigma \frac{\sigma(\boldsymbol{q}, \boldsymbol{r}_0, s)\,(\boldsymbol{p}-\boldsymbol{q})\cdot\boldsymbol{n}(\boldsymbol{p})}{|\boldsymbol{p}-\boldsymbol{q}|^3}\,\mathrm{d}S(\boldsymbol{q}). \tag{5.7}$$

A particular difficulty with this equation is the singularity in the integrand at $\boldsymbol{q} = \boldsymbol{p}$; however, this can be removed (Landweber & Shahshahan 1992) by noting that

$$\int_\Sigma \frac{(\boldsymbol{p}-\boldsymbol{q})\cdot\boldsymbol{n}(\boldsymbol{q})}{|\boldsymbol{p}-\boldsymbol{q}|^3}\,\mathrm{d}S(\boldsymbol{q}) = 2\pi. \tag{5.8}$$

Then (5.7) may be written as

$$\sigma(\boldsymbol{p}, \boldsymbol{r}_0, s) = \frac{1}{4\pi}\frac{(\boldsymbol{p}-\boldsymbol{r}_0)\cdot\boldsymbol{n}(\boldsymbol{p})}{|\boldsymbol{p}-\boldsymbol{r}_0|^3} + \frac{1}{4\pi}\int_\Sigma \frac{\{\sigma(\boldsymbol{q}, \boldsymbol{r}_0, s)\,(\boldsymbol{p}-\boldsymbol{q})\cdot\boldsymbol{n}(\boldsymbol{p}) - \sigma(\boldsymbol{p}, \boldsymbol{r}_0, s)\,(\boldsymbol{q}-\boldsymbol{p})\cdot\boldsymbol{n}(\boldsymbol{q})\}}{|\boldsymbol{p}-\boldsymbol{q}|^3}\,\mathrm{d}S(\boldsymbol{q}). \tag{5.9}$$

Equation (5.9) is a Fredholm integral equation of the second kind and provided the process converges, may be solved by iteration as follows:

$$\sigma^{(0)}(\boldsymbol{p}, \boldsymbol{r}_0, s) = \frac{1}{4\pi}\frac{(\boldsymbol{p}-\boldsymbol{r}_0)\cdot\boldsymbol{n}(\boldsymbol{p})}{|\boldsymbol{p}-\boldsymbol{r}_0|^3}, \tag{5.10}$$

$$\sigma^{(n)}(\boldsymbol{p}, \boldsymbol{r}_0, s) = \sigma^{(0)}(\boldsymbol{p}, \boldsymbol{r}_0, s) + \frac{1}{4\pi}\int_\Sigma \frac{\{\sigma^{(n-1)}(\boldsymbol{q}, \boldsymbol{r}_0, s)\,(\boldsymbol{p}-\boldsymbol{q})\cdot\boldsymbol{n}(\boldsymbol{p}) - \sigma^{(n-1)}(\boldsymbol{p}, \boldsymbol{r}_0, s)\,(\boldsymbol{q}-\boldsymbol{p})\cdot\boldsymbol{n}(\boldsymbol{q})\}}{|\boldsymbol{p}-\boldsymbol{q}|^3}\,\mathrm{d}S(\boldsymbol{q}), \tag{5.11}$$

where the superscript $(n)$ denotes the approximation obtained by performing $n$ iterations of (5.10) and (5.11). The particular numerical details in carrying out this iteration may vary depending upon the particular geometry.

To illustrate one approach, the specific example where $\Sigma$ is a body of revolution about the $x$-axis will be considered in detail. The flow domain is infinite and the position of the body fixed. The surface of the body is given in parametric form as a function of $\xi$ and $\theta$ as

$$\boldsymbol{p} = (X(\xi), \tau(\xi)\sin\theta, \tau(\xi)\cos\theta), \tag{5.12}$$

where $\theta$ is measured from the vertical. The variable $\xi$ is the arclength along the curve that generates the body. The radius of the body, $\tau$, may be equivalently considered as a function of $X$, in which case it is evident that

$$\xi = \int_0^X (1+\tau_X^2(X'))^{\frac{1}{2}}\,\mathrm{d}X', \tag{5.13}$$

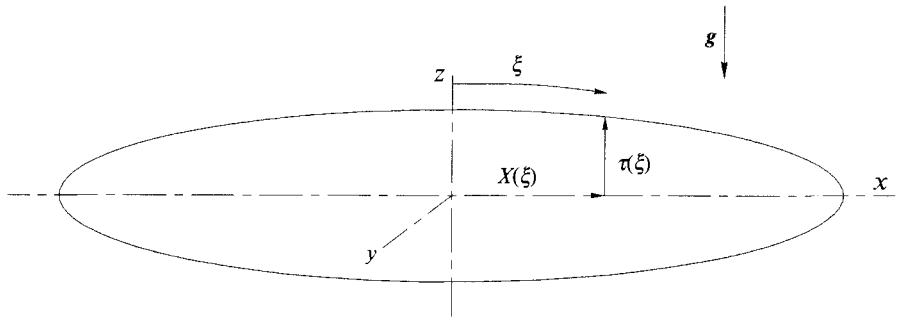


FIGURE 4. The geometry of a body of revolution.

the subscript $X$ denoting differentiation. The geometry is shown in figure 4 and as a consequence of the parameterization with respect to $\xi$,

$$X_\xi^2+\tau_\xi^2=1. \tag{5.14}$$

Axisymmetry may be exploited here in the evaluation of $\Gamma$ and $\mu$, so inception is considered to occur at

$$\boldsymbol{r}_0=(\zeta,0,\omega). \tag{5.15}$$

The unit normal to $\Sigma$, exterior to the flow domain is given by

$$\boldsymbol{n}=(\tau_\xi,-X_\xi\sin\theta,-X_\xi\cos\theta), \tag{5.16}$$

and the surface area element is

$$\mathrm{d}S=\tau\,\mathrm{d}\theta\,\mathrm{d}\xi. \tag{5.17}$$

Using (5.12) and (5.15)–(5.17) in (5.9) yields

$$\begin{aligned}\sigma(\xi,\theta)=\frac{1}{4\pi}\frac{\omega X_\xi(\xi)\cos(\theta)+\tau_\xi(\xi)(X(\xi)-\zeta)-\tau(\xi)X_\xi(\xi)}{((X(\xi)-\zeta)^2+\omega^2-2\omega\tau(\xi)\cos(\theta)+\tau^2(\xi))^{\frac{3}{2}}}+\frac{1}{4\pi}\int_{\xi_{min}}^{\xi_{max}}\mathrm{d}\xi'\int_0^{2\pi}\mathrm{d}\theta'\,\tau(\xi')\\ \times[\sigma(\xi',\theta')\{(X(\xi)-X(\xi'))\tau_\xi(\xi)-X_\xi(\xi)\tau(\xi)+X_\xi(\xi)\tau(\xi')\cos(\theta-\theta')\}\\ -\sigma(\xi,\theta)\{(X(\xi')-X(\xi))\tau_\xi(\xi')-X_\xi(\xi')\tau(\xi')+X_\xi(\xi')\tau(\xi)\cos(\theta-\theta')\}]/\\ [(X(\xi)-X(\xi'))^2+\tau^2(\xi)+\tau^2(\xi')-2\tau(\xi)\tau(\xi')\cos(\theta-\theta')]^{\frac{3}{2}}.\end{aligned} \tag{5.18}$$

Symmetry about the plane $y=0$ is exploited in order to reduce the interval of $\theta'$ integration to $[0,\pi]$. The interval $[\xi_{min},\xi_{max}]$ is partitioned into $n_\xi$ segments by the sequence $\{\xi_1,\xi_2,\ldots,\xi_{n_\xi+1}\}$. Similarly, $[0,\pi]$ is partitioned into $n_\theta$ segments by the sequence $\{\theta_1,\theta_2,\ldots,\theta_{n_\theta+1}\}$. Notice that $\xi_1=\xi_{min}$, $\xi_{n_\xi+1}=\xi_{max}$, $\theta_1=0$ and $\theta_{n_\theta+1}=\pi$. The following quantities are also defined:

$$\left.\begin{aligned}\delta\xi_{i+1}&=\xi_{i+1}-\xi_i,\quad i=1,2,\ldots,n_\xi,\\ \delta\theta_{j+1}&=\theta_{j+1}-\theta_j,\quad j=1,2,\ldots,n_\theta.\end{aligned}\right\} \tag{5.19}$$

This division defines a mesh over $[\xi_{min},\xi_{max}]\times[0,\pi]$ which consists of $n_\xi n_\theta$ rectangular elements. Element $i,j$ has vertices $(\xi_i,\theta_j)$, $(\xi_{i+1},\theta_j)$, $(\xi_{i+1},\theta_{j+1})$, $(\xi_i,\theta_{j+1})$.

The iteration of (5.18) following (5.10) and (5.11) is carried out at a set of $n_\xi n_\theta$ nodes defined by

$$(\xi_{i+\frac{1}{2}},\theta_{j+\frac{1}{2}})=(\xi_i+\tfrac{1}{2}\delta\xi_{i+1},\theta_j+\tfrac{1}{2}\delta\theta_{j+1}),\quad i=1,2,\ldots,n_\xi,\quad j=1,2,\ldots,n_\theta. \tag{5.20}$$

In order to perform the integration over element $i,j$ in (5.18), the source density $\sigma$ is assumed constant and equal to $\sigma_{ij}$, its value at $(\xi_{i+\frac{1}{2}},\theta_{j+\frac{1}{2}})$. A product Gauss rule is

employed with an even number of abscissae, in order that no Gaussian point coincides with a node point. In order to evaluate $\tau$, $X$, $\tau_\xi$ and $X_\xi$ at the Gaussian points, a cubic spline is used to approximate $\tau(\xi)$ and $X(\xi)$ and constrained to pass through the values of these functions at $\xi_i\{i = 1, 2, \ldots, n_\xi + 1\}$. Evaluating (5.18) utilizing these representations yields the equation

$$\sigma_{ij}^{(n)} = \sigma_{ij}^{(0)} + \sum_{k=1}^{n_\xi} \sum_{l=1}^{n_\theta} G_{ijkl}\, \sigma_{kl}^{(n-1)}, \tag{5.21}$$

with

$$G_{ijkl} = \frac{1}{4\pi} \sum_{\alpha=1}^{2} \sum_{i_\xi=1}^{n_{g\xi}} \sum_{i_\theta=1}^{n_{g\theta}} w_{k,i_\xi} w_{l,i_\theta} \tau(\xi_{k,i_\xi})$$

$$\times \frac{[(X(\xi_{i+\frac{1}{2}}) - X(\xi_{k,i_\xi}))\,\tau_\xi(\xi_{i+\frac{1}{2}}) - X_\xi(\xi_{i+\frac{1}{2}})\,\tau(\xi_{i+\frac{1}{2}}) + X_\xi(\xi_{i+\frac{1}{2}})\,\tau(\xi_{k,i_\xi})\cos(\theta_{j+\frac{1}{2}} + (-1)^\alpha \theta_{l,i_\theta})]}{[(X(\xi_{i+\frac{1}{2}}) - X(\xi_{k,i_\xi}))^2 + \tau^2(\xi_{i+\frac{1}{2}}) + \tau^2(\xi_{k,i_\xi}) - 2\tau(\xi_{i+\frac{1}{2}})\,\tau(\xi_{k,i_\xi})\cos(\theta_{j+\frac{1}{2}} + (-1)^\alpha \theta_{l,i_\theta})]^{\frac{3}{2}}}$$

$$-\frac{1}{4\pi}\delta_{ik}\,\delta_{jl} \sum_{\alpha=1}^{2} \sum_{k=1}^{n_\xi} \sum_{l=1}^{n_\theta} \sum_{i_\xi=1}^{n_{g\xi}} \sum_{i_\theta=1}^{n_{g\theta}} w_{k,i_\xi} w_{l,i_\theta} \tau(\xi_{k,i_\xi})$$

$$\times \frac{[(X(\xi_{k,i_\xi}) - X(\xi_{i+\frac{1}{2}}))\,\tau_\xi(\xi_{k,i_\xi}) - X_\xi(\xi_{k,i_\xi})\,\tau(\xi_{k,i_\xi}) + X_\xi(\xi_{k,i_\xi})\,\tau(\xi_{i+\frac{1}{2}})\cos(\theta_{j+\frac{1}{2}} + (-1)^\alpha \theta_{l,i_\theta})]}{[(X(\xi_{i+\frac{1}{2}}) - X(\xi_{k,i_\xi}))^2 + \tau^2(\xi_{i+\frac{1}{2}}) + \tau^2(\xi_{k,i_\xi}) - 2\tau(\xi_{i+\frac{1}{2}})\,\tau(\xi_{k,i_\xi})\cos(\theta_{j+\frac{1}{2}} + (-1)^\alpha \theta_{l,i_\theta})]^{\frac{3}{2}}}. \tag{5.22}$$

In this expression, $n_{g\xi}$ and $n_{g\theta}$ respectively denote the number of Gaussian points used to carry out the integration over $\xi'$ and $\theta'$, $w_{k,i_\xi}$ and $w_{l,i_\theta}$ denote the weights and $\xi_{k,i_\xi}$ and $\theta_{l,i_\theta}$ the abscissae for integration over the element $k$, $l$. $\delta_{ik}$ is the Kronecker delta, as is $\delta_{jl}$.

To test and illustrate the numerical method, consider the oblate spheroid given by revolution of the curve

$$X^2 + \tau^2/\eta^2 = \ell^2, \tag{5.23}$$

about the $x$-axis, with $\eta \leqslant 1$. The case $\eta = 1$ is a sphere and comparison with the exact solution presented in the previous section allows the numerical scheme to be validated. In order to partition the interval $[\xi_{min}, \xi_{max}]$, points are chosen as

$$\left.\begin{aligned} X_i = \ell \sin(\psi_i), \quad \tau_i = n\ell \cos(\psi_i), \\ \psi_i = -\tfrac{1}{2}\pi + (i-1)\,\pi/n_\xi, \quad i = 1, 2, \ldots, n_\xi + 1. \end{aligned}\right\} \tag{5.24}$$

A cubic spline is fitted to these points using the technique of Kucera (1993) that yields the parameterization with respect to the exact arclength $\xi$. A particular benefit of utilizing (5.24) to partition $[\xi_{min}, \xi_{max}]$ is that, in the case where the body is slender, smaller elements are chosen near the ends where the curvature is high. In this example $\delta\theta_{j+1} = \delta\theta$ is a constant.

The performance of the numerical method in the case of a sphere of radius 1 is illustrated by figure 5(*a*, *b*). Figure 5(*a*) shows the relative error in $\Gamma_r$, the non-zero component of $\boldsymbol{\Gamma}$ directed towards the centre of the sphere, and figure 5(*b*) shows the relative error in $\mu$. The variation of the error with $\xi$, the distance of the inception point from the centre of the sphere, is shown for various $n_\xi \times n_\theta$ combinations, in particular $14 \times 14$, $19 \times 19$, $24 \times 24$, $29 \times 29$ and $34 \times 34$. In all computations $n_{g\xi} = n_{g\theta} = 2$ and (5.21) was iterated until the solution had converged in the sixth decimal place. This required approximately 7 to 15 iterations, the larger number when $\xi \approx 1$. These graphs display the convergence of the method as the mesh is refined. Furthermore, they

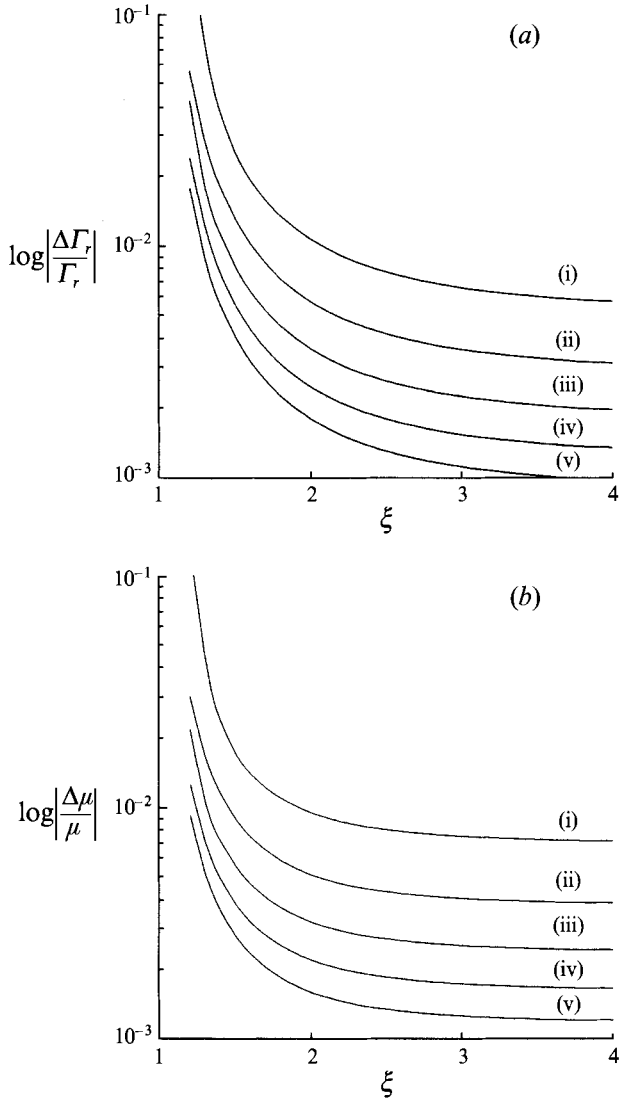


FIGURE 5. The relative error in calculation of (*a*) $\Gamma_r$ and (*b*) $\mu$ for the example of a sphere of radius 1. The variation of this error with $\xi$ is shown for the mesh sizes: (i) $14 \times 14$, (ii) $19 \times 19$, (iii) $24 \times 24$, (iv) $29 \times 29$, (v) $34 \times 34$.

illustrate the divergence as $\xi \to 1$. This corresponds to the point of inception approaching the sphere surface and in view of this interpretation it is evident that the numerical calculation should diverge under these circumstances. If calculations were required to very high accuracy in the event of $\xi \approx 1$, the method could be improved by noting that in such a case the flow field in the neighbourhood of the bubble source appears as for a source near a plane boundary, an example for which the solution is known. Alternatively, a mesh refinement process could be utilized. However, the validity of the theory is questionable in such a regime so it does not seem appropriate to invest a great deal of effort in highly accurate calculations there.

The numerical method for calculation of $\boldsymbol{\Gamma}$ and $\mu$ may be used to compute the zone of attraction around various bodies, just as was done for the example of a sphere. The zone of attraction around the sphere shown in figure 2 was calculated using the

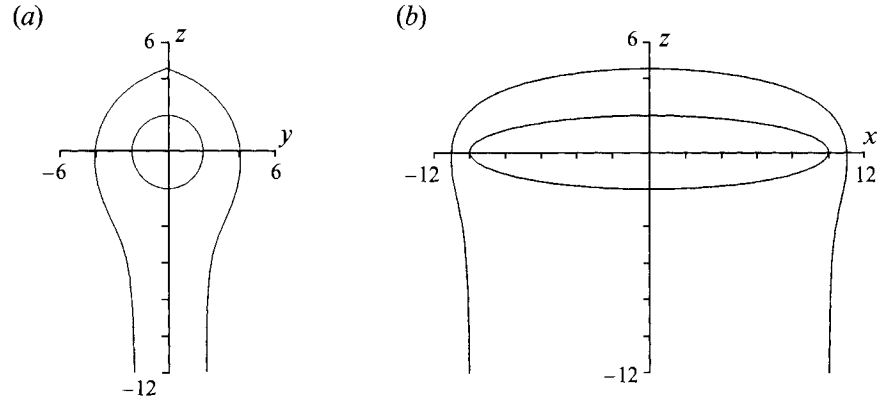


FIGURE 6. The zone of attraction around the body of revolution defined by (5.23), $l = 10$, $\eta = 0.2$, $\delta = 0.1$. The cross-sections through the planes (*a*) $x = 0$ and (*b*) $y = 0$ are shown.

numerical method employing $n_\xi = n_\theta = 14$ and 10 iterations of (5.21). The result was visually indistinguishable from that computed using the analytical expressions. Since the smallest value $\xi/a$ takes is about 2, inspection of figure 5(*a*, *b*) reveals that both $\Gamma_r$ and $\mu$ are computed with a relative error of less than $10^{-2}$, and this has proved to be entirely sufficient.

As an example relevant to the problem of underwater explosion bubble collapse near a marine vessel, consider the zone of attraction about the body defined by (5.23) in an infinite fluid, with a uniform gravitational field acting. The geometry of $S_a$, in the planes $x = 0$ and $y = 0$, is shown in figure 6 for the case $\ell = 10$, $\eta = 0.2$ and $\delta = 0.1$. In this example $n_\xi = 19$, and $n_\theta = 14$ with ten iterations of (5.21) carried out. As for collapse near a sphere, as $z \to -\infty$ the section of $S_a$ in the plane $z =$ constant tends to the section of the body in the plane $z = 0$.

In concluding this section, it is noted that the CPU time required to compute an approximation to the Kelvin impulse using the technique described here is less than the time taken to perform one time iteration of a boundary integral calculation of the whole flow field (see for example Harris 1992). This provides an illustration of the power of this theory. An estimate of the important parameter of the direction of jet formation upon transient cavity collapse may be made with considerable economy in some rather complex but practically relevant geometries.

## 6. Conclusions

In this paper, an expression has been given that relates the components of the Bjerknes force acting on a bubble to the singularities of the fluid velocity potential within the bubble, defined there by analytic continuation. Application of this expression to transient cavities allows a general theory to be developed for estimating the Kelvin impulse during collapse in a flow field of general geometry, assuming that perturbations from spherical shape are small. Since the large deformation from a spherical shape brought about by jet formation occurs quickly, the estimates obtained assuming small departures from a spherical shape are expected to well approximate the impulse of the cavity after jet formation has occurred. Using this theory, the result of Blake *et al.* (1986) for the impulse of a cavity collapsing near a plane rigid boundary has been recovered, and the effort required in carrying out the analysis is significantly less than for the original approach.

The power of the general theory has been illustrated by consideration of the further examples of transient cavity collapse near a sphere, both in an infinite fluid and partially submerged at a horizontal free surface. Furthermore, a numerical implementation of the method has been illustrated that allows complex flow field geometries to be considered. Since the direction of jet formation upon the collapse of a transient cavity appears to be correlated with the direction of the Kelvin impulse, the analytical and numerical estimates obtained for the impulse may be used to predict the direction of jet formation. In this context the concept of a zone of attraction surrounding an isolated body has been introduced. If inception of a cavity occurs in this region of the flow domain, the final Kelvin impulse (and presumably the jet) will be directed towards the body. The bounding surface of this region may be calculated using the estimates of the final Kelvin impulse computed in this paper.

Significant assumptions have been made in developing the theory of this paper, as stated above. However, the evidence obtained to date, particularly from numerical simulations, indicates that the results derived here provide a reliable indicator of jetting behaviour upon the collapse of transient cavities. The numerical simulations of Blake *et al.* (1986, 1987) indicate well the qualitative correlation between the directions of the Kelvin impulse at collapse and the jet. These results further indicate that analytical approximations derived assuming that $\epsilon$ is small still provide reasonable predictions of jetting behaviour when inception of a transient cavity occurs at approximately one maximum bubble radius from a rigid boundary or, in the notation of this paper, when $\epsilon$ is $O(1)$. As a further comment, cavity collapse near a compliant boundary has been considered briefly by Blake (1988), and the analytical estimate of the final Kelvin impulse provides predictions of jetting behaviour that are in accord with the scarce experimental data available.

In order to determine fully the realms of applicability of the theory developed here, further experimental and numerical work is required. Both are currently proceeding, especially addressing cavity collapse in the neighbourhood of the non-trivial geometries considered here.

We would like to thank an anonymous referee whose constructive comments have contributed to a substantially improved final manuscript.

## REFERENCES

ABRAMOWITZ, M. & STEGUN, I. A. 1965 *Handbook of Mathematical Functions*. Dover.

BENJAMIN, T. B. & ELLIS, A. T. 1966 The collapse of cavitation bubbles and the pressures thereby produced against solid boundaries. *Phil. Trans. R. Soc. Lond.* A **260**, 221–240.

BLAKE, J. R. 1988 The Kelvin impulse: Application to cavitation bubble dynamics. *J. Austral. Math. Soc.* B **30**, 127–146.

BLAKE, J. R. & CERONE, P. 1982 A note on the impulse due to a vapour bubble near a boundary. *J. Austral. Math. Soc.* B **23**, 383–393.

BLAKE, J. R., TAIB, B. B. & DOHERTY, G. 1986 Transient cavities near boundaries. Part 1. Rigid boundary. *J. Fluid Mech.* **170**, 479–497.

BLAKE, J. R., TAIB, B. B. & DOHERTY, G. 1987 Transient cavities near boundaries. Part 2. Free surface. *J. Fluid Mech.* **181**, 197–212.

GRADSHTEYN, I. S. & RYZHIK, I. M. 1979 *Tables of Integrals, Series and Products*. Academic.

GUERRI, L., LUCCA, G. & PROSPERETTI, A. 1981 A numerical method for the dynamics of non-spherical cavitation bubbles. In *Proc. 2nd Intl Colloq. on Drops and Bubbles, Monterey, California*, JPL Publication 82-7, pp. 175–181.

HARRIS, P. J. 1992 A numerical model for determining the motion of a bubble close to a fixed rigid structure in a fluid. *Intl J. Numer. Methods Engng* **33**, 1813–1822.

HERRING, C. 1950 Theory of the pulsations of the gas bubble produced by an underwater explosion. In *Underwater Explosion Research*, Vol. II (ed. G. K. Hartmann & E. G. Hill). Office of Naval Research, Washington, D.C.

KUCERA, A. 1993 A boundary integral method applied to the growth and collapse of bubbles near a rigid boundary. *J. Comput. Phys.* (submitted).

LANDWEBER, L. & MILOH, T. 1980 Unsteady Lagally theorem for multipoles and deformable bodies. *J. Fluid Mech.* **96**, 33–45.

LANDWEBER, L. & SHAHSHAHAN, A. 1992 Added masses and forces on two bodies approaching central impact in an inviscid fluid. *J. Ship Res.* **36**, 99–122.

LAUTERBORN, W. & BOLLE, H. 1975 Experimental investigations of cavitation bubble collapse in the neighbourhood of a solid boundary. *J. Fluid Mech.* **72**, 391–399.

MILNE-THOMSON, L. M. 1960 *Theoretical Hydrodynamics*. Macmillan.

NEWMAN, J. N. 1977 *Marine Hydrodynamics*. MIT Press.

PLESSET, M. S. & CHAPMAN, R. B. 1971 Collapse of an initially spherical vapour cavity in the neighbourhood of a solid boundary. *J. Fluid Mech.* **47**, 283–290.

RAYLEIGH, LORD 1917 On the pressure developed in a liquid during the collapse of a spherical void. *Phil. Mag.* **34**, 94–98.

VOGEL, A., LAUTERBORN, W. & TIMM, R. 1989 Optical and acoustic investigations of the dynamics of laser-produced cavitation bubbles near a solid boundary. *J. Fluid Mech.* **206**, 299–338.